Proceedings of the 9th International and 49th National Conference on Fluid Mechanics and Fluid Power (FMFP)
December 14-16, 2022, IIT Roorkee, Roorkee-247667, Uttarakhand, India

FMFP2022–XX–YYY

Numerically Optimized Thermal Modeling of Fluid Flow and Heat Transfer in Direct Contact Membrane Distillation

Khushwant Singh Chauhan[1], and Himanshu Tyagi[1]

[1]Department of Mechanical Engineering, IIT Ropar, Rupnagar, Punjab - 140001, India

ABSTRACT

The present study defines the mathematical model, and a numerical study is conducted to get the approximate results using the conservation of mass and energy. These properties are then calculated, and variations in input parameters like membrane properties, flow rate, flow type, Reynolds number, concentration, and climate effect are varied to get optimum results. Various studies have been conducted at TDS of 10 PPT, and we have identified that the polyvinylidene fluoride (PVDF) membrane provides the highest permeate water flux. It is also seen that when the flow changes from laminar to turbulent, at the transition zone, we get the highest permeate water flux, but it keeps on increasing with increased Reynolds number in the turbulent region, but it is not advisable to go beyond the transition phase; otherwise, it will increase the heat loss due to high turbulence eddies formation, and also, we need more power supply to increase Reynolds number; hence further studies are carried out at Reynolds number of 2100. One thing is also observed that a country with a high annual average temperature will produce high permeate water flux.

Keywords: Membrane Distillation, Desalination, Fluid flow, Heat Transfer, Mass Transfer, Solar Energy.

1. INTRODUCTION

Presently around 1.42 billion people, including children of a total of 450 million, live in highly water-prone areas. By 2050, global water consumption is projected to increase by 20 to 30% annually [1]. Freshwater availability is less than 3% of the world's total water supply, which is becoming harder. Water stress is increasing by years of water mismanagement, excessive groundwater extraction, and pollution of freshwater sources. The freshwater requirement is increasing due to urbanization, fast population increase, and growing demands from various industries, most notably agriculture, industry, and energy. Desalination of water is one of the ways to convert non-potable water into potable water. In DCMD, the flow of hot side feed saline water and cold side permeate distilled water are separated by a microporous hydrophobic membrane. Due to the flow of hot feed and cold permeate, the membrane surface gets heated on one of the membrane surfaces, and it gets cooled at another membrane surface, which eventually creates the temperature difference between membrane surfaces resulting in the generation of a vapor pressure difference which acts as the driving force that transports the vapor of water through a membrane and, it gets converted into distilled water. The vapor pressure difference is the function of various parameters like bulk feed and permeates inlet temperature, design of the module, type of flow, feed mass flow rate, etc.

MD is an energy-efficient desalination process with lots of potential compared to the conventional desalination process (i) low operating temperature requirement, (ii) low operating vapor pressure, (iii) high rejection (100% theoretical) of ions, colloids, non-volatiles, macro-molecules, (iv) use low-grade energy [2]. Due to its common temperature requirement, we can use industrial waste energy, low-grade energy, geothermal energy, solar energy, etc. In our system, we use solar energy, which is readily available in most developing countries. We can set up a solar-based DCMD system in a rural area, making this system portable and reliable for getting fresh water. MD system can also be integrated with other systems like reverse osmosis (RO) [3], ultrafiltration (UF) [4], or humidification-dehumidification (HDH) system.

2. LITERATURE REVIEW AND OBJECTIVE

Membrane distillation (MD) is one of the thermal-driven methods which produce distilled water from saline water across the membrane due to temperature difference between hot and cold flow, as the membrane distillation process operates at a lower temperature compared to RO; hence low-grade energy, geothermal energy, and renewable energy (such as solar) can be used to make desalination affordable without significantly affecting the environment.

It is observed that in an MD system, the permeate water flux depends on the characteristic of membranes, like liquid entry pressure, pore size, membrane thickness, porosity, tortuosity, and pore distribution. The membrane should be non-wetting with low thermal conductivity, high thermal stability at elevated temperatures, low mass transfer resistance, good chemical resistance, etc. [5]. There exists various types of membrane module like hollow fiber, spiral wounded, tubular membrane, and flat sheet membrane, but the flat or plate type membrane is the most popular and widely used membrane module in desalination of saline water, it is because it is more straightforward in design and the permeate water flux obtained is high compared to other membrane module design. The temperature distribution is done by doing the numerical mathematical modeling using €-NTU methods, which are generally used in the heat exchanger, DCMD also behaves similar to the heat exchanger, but the aim here is to reduce the

heat loss and increase the mass transfer; therefore, the module is designed in such a manner that the heat transfer (HT) from the module can be reduced. The heat exchanger approach is used in which we performed the counter flow of feed saline water and permeated distilled water; the counter flow is selected to reduce the area of the membrane module and compact the system. The variation in temperature profile in counterflow is not linear. Still, for simplification, we will use a linear profile so that the temperature profile of the membrane, the temperature profile of feed saline water, and permeate distilled water variation along the length of the membrane can be evaluated using the interpolation method.

The objective is to find out optimum permeate water flux by performing the variation in membrane properties, like porosity, pore size, membrane thickness, etc., operating parameters like the atmospherical condition of different locations, effect on permeate water flux by changing the mass flow rate of feed, feed velocity, or by changing the type of flow like laminar or turbulent.

3. MATERIALS AND METHODS

3.1 Fluid Properties and Materials used

The fluids properties of the feed and permeates side. For simplification, we assumed the properties of the fluids like density, dynamic viscosity, specific heat, and Prandtl number for feed and permeate side to be constant, which is 1000 (kgm^{-3}), 0.001(Nsm^{-2}), 4182($Jkg^{-1}K^{-1}$), and 6.9 respectively. Still, the thermal conductivity of saline water at specified temperatures and salinity is considered, and it varies between 0.572 – 0.682 (W/m-K) [6]. We are using three membranes for our study purpose, and their characteristics are provided in table 1 [7–10].

Table 1: Characteristics of membranes [7–10].

Membrane	Porosity (-)	Pore size	Thickness
PTFE	0.7	0.25 (µm)	100 (µm)
PP	0.55	0.064 (µm)	150 (µm)
PVDF	0.78	0.98 (µm)	82 (µm)

3.2 Numerical mathematical modeling

Figure 1 shows the schematic of DCMD. As the fluids initially flow on the feed side and permeate side, there is a formation of thermal and hydrodynamic boundary layer; after that, they both attend the fully developed region, and flow becomes steady. The module design cannot be made perfectly insulated; hence heat loss takes place; because of the formation of the temperature boundary layer, therefore, there exists a difference in feed bulk and membrane temperature, which is one of the disadvantages of DCMD that there is a loss in driving force between feed and permeates side, and this loss of temperature is temperature polarization, and the factor which tells us how much heat loss takes palace is the coefficient of temperature polarization (φ) which is defined as [8]:

$$\varphi = \frac{T_{fm} - T_{pm}}{T_{fb} - T_{pb}} \quad (1)$$

φ varies from zero to one, and getting the value close to one is preferable. The feed and permeate membrane temperature is evaluated using the heat balance and conversation laws.

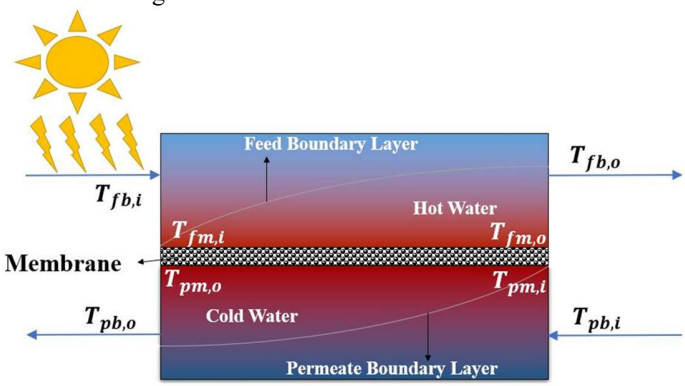

Figure 1: Schematic of Solar-based DCMD

3.3 Analysis of mass transfer

Darcy's law describes the mass transport over the microporous hydrophobic membrane in DCMD [11]:

$$J_{pw} = B_{mmt}\left(P_{v,f} - P_{v,p}\right) \quad (2)$$

where B_{mmt} is dependent upon various parameters like geometric parameters like porosity, ε (-), tortuosity, τ (-), pore radius, r_p (m), membrane thickness, δ (m), and operating parameters like average membrane temperature, $T_{avg,m}$ (K), the molecular weight of solute, M (g/mol), membrane air pressure, $P_{m,air}$ (Pa). B_{mmt} is calculated by assuming the pore to be a uniform cylindrical shape [8]. Antoine equation is used to calculate the vapor pressure of feed and permeate [7].

$$P_v = exp\left(23.238 - \frac{3841}{T_m - 45}\right) \quad (3)$$

Feed is a mixture of pure water and salt; hence, we use Raoult's law to evaluate the vapor pressure of feed which is given by:

$$P_{v,f} = \left(1 - X_{solute}\right) * P_{v,pure-solvent} \quad (4)$$

The dusty gas model (DGM) [8] suggested that the diffusion mass transport mechanism is categorized into three regions due to collisions between membrane and/or between molecules (i) Knudsen region, (ii) Continuum region, and (iii) transition region according to DGM. The dominant diffusion mass transport mechanism in DCMD is classified according to the value of the Knudsen number (κ_n) [2].

$$\kappa_n = \frac{\lambda}{D_p} \quad (5)$$

When $\kappa_n > 1$ (i.e., $D_p <$ λ,). The mass transport mode is Knudsen diffusion and the region Knudsen region. For that B_{mmt} is given by Qtaishat et al. [8]

$$B_{mmt} = \frac{2\varepsilon r_p}{3\tau\delta}\left(\frac{8\mathrm{RT_{avg,m}}}{\pi M}\right)^{1/2}\frac{M}{\mathrm{RT_{avg,m}}} \quad (6)$$

When $0.01 < \kappa_n < 1$ (i.e., $\lambda < d_p < 100\lambda$,). The mass transport mode is a combination of Molecular and Knudsen Diffusion, and the region is the Transition region. For that B_{mmt} is given by Qtaishat et al. [8]

$$B_{mmt} = \left[\frac{2\varepsilon r_p}{3\tau\delta}\left(\frac{\pi\mathrm{RT_{avg,m}}}{8M}\right)^{1/2} + \frac{\tau\delta P_{m,air}R\mathrm{T_{avg,m}}}{\varepsilon P_T D_w M}\right]^{-1} \quad (7)$$

The product of total pressure of water vapor/air and diffusion coefficient of water ($P_T D_w$) is evaluated from the given expression [12].

$$P_T D_w = (1.895T^{2.072}) * 10^{-5} \quad (8)$$

When $\kappa_n < 0.01$ (i.e., $D_p > 100\ \lambda$,). The mass transport mode is ordinary molecular diffusion, and the region is the Continuum region. For that B_{mmt} is given by [8]:

$$B_{mmt} = \frac{\varepsilon P_T D_w M}{\tau\delta P_{m,air}R\mathrm{T_{avg,m}}} \quad (9)$$

3.4 Analysis of heat transfer

In DCMD, heat transfer takes palace due to temperature difference, and heat transfer due to mass transport of vapor is classified into three regions (i) feed side convective heat transfer and HT due to transport of vapor due to temperature boundary layer (ii) conductive heat transfer in membrane and latent HT associated with vapor flux and (iii) permeate side convective heat transfer and HT due to transport of vapor due to temperature boundary layer. The enthalpy in the vapor phase is much higher than the enthalpy in the liquid region [13]. Qtaishat et al. [8] found that heat transfer due to water vapor transport in feed and permeate sides are 4.3% and 1.43% of total heat transfer, respectively, and therefore for simplification, we can neglect the enthalpy of feed and permeate, i.e.,,, liquid region enthalpy; hence we can tell that on feed and permeate sides convection phenomenon is dominating, and simplified heat equation can be written as follows:

$$Q_{T,f} = h_f A_m\left(T_{fb} - T_{fm}\right) \quad (10)$$

$$Q_{T,m} = \frac{K_m A_m\left(T_{fm} - T_{pm}\right)}{\delta} + J_{pw}A_m H_{m,v} \quad (11)$$

$$Q_{T,p} = h_p A_m\left(T_{pm} - T_{pb}\right) \quad (12)$$

The thermal conductivity of the membrane is evaluated using the mathematical relation given by Alkhudhiri et al. [5]:

$$K_m = (1-\varepsilon)K_p + \varepsilon K_a \quad (13)$$

The enthalpy of water vapor on the membrane is evaluated using the mathematical relation given by [14]:

$$H_{m,v} = 1.7535T_{avg,m} + 2024.3 \quad (14)$$

The heat transfer coefficient on the feed and permeate side is evaluated using the Nusselt number relation, which is given by [13]:

$$Nu_f = \frac{h_f D_h}{K_f}, \quad Nu_p = \frac{h_p D_h}{K_p} \quad (15)$$

In order to evaluate the Nusselt number (Nu), we need to know about the Reynolds number (Re) and the hydraulic diameter, (D_h) of the flow channel is given by [13]:

$$\mathrm{Re} = \frac{\rho v D_h}{\mu}, \quad D_h = \frac{4A_m}{W_m} \quad (16)$$

Table 2: Nusselt number correlation for evaluating heat transfer coefficient [12,14]

Type of flow	Correlation used	Equation
Laminar	$\mathrm{Nu} = 3.36 + \frac{0.036\mathrm{RePr}\frac{D_h}{L}}{1 + 0.0011\left(\mathrm{RePr}\frac{D_h}{L}\right)^{0.8}}$	(17)
Turbulent	$\mathrm{Nu} = 0.023\left(1 + \frac{6D_h}{L}\right)\mathrm{Re}^{0.8}\mathrm{Pr}^{1/3}$	(18)

During the steady state conditions $Q_{T,f} = Q_{T,m} = Q_{T,p} = Q$
Now, by applying energy balance, the feed and permeate membrane temperature can be written as follows:

$$T_{fm} = \frac{T_{pb} + \left(\frac{h_f}{h_p}\right)T_{fb} + \frac{\delta}{K_m}\left[h_f T_{fb} - J_{pw}H_{m,v}\right]}{1 + \frac{\delta h_f}{K_m} + \frac{h_f}{h_p}} \quad (19)$$

$$T_{pm} = \frac{T_{fb} + \left(\frac{h_p}{h_f}\right)T_{pb} + \frac{\delta}{K_m}\left[h_p T_{pb} + J_{pw}H_{m,v}\right]}{1 + \frac{\delta h_p}{K_m} + \frac{h_p}{h_f}} \quad (20)$$

3.4.1 Effectiveness-NTU method

We are using the $€ - NTU$ method to get the variation of the temperature profile in the bulk, feed, bulk membrane, and feed membrane. Heat transfer along the length of the membrane using energy balance is given by [13]:

$$Q = C_{p,f}\left(T_{fb,i} - T_{fb,o}\right) = C_{p,p}\left(T_{pb,i} - T_{pb,o}\right) \quad (21)$$

For evaluating the outlet of feed and permeate bulk temperature, we are using the $€ - NTU$ method, and effectiveness is given by [13]:

$$€ = \frac{C_{p,f}\left(T_{fb,i} - T_{fb,o}\right)}{C_{min.}\left(T_{fb,i} - T_{pb,i}\right)} = \frac{C_{p,p}\left(T_{pb,i} - T_{pb,o}\right)}{C_{min.}\left(T_{fb,i} - T_{pb,i}\right)} \quad (22)$$

The overall heat transfer coefficient and NTU are given below by equation (23) [15]:

$$\frac{1}{U} = \frac{1}{h_f} + \frac{\delta}{K_m} + \frac{1}{h_p}, \quad NTU = \frac{UA_m}{C_{min.}} \tag{23}$$

Combining equations (22) and (23), the expression of effectiveness becomes that is given in equation (24), and for simplification, we are taking the mass flow rate of feed and permeate to be identical and assuming specific heat of permeate and feed side to be equal, which caused the unit capacity ratio, and for unit capacity ratio, effectiveness is given by [13]:

$$€ = \frac{1-exp(-NTU(1-C_r))}{1-C_r.exp(-NTU(1-C_r))}, \quad € = \frac{NTU}{NTU+1} \tag{24}$$

3.4.2 Entry length

Hydrodynamic entry length tells us when the fluid velocity became constant along the length of the flow, i.e., became fully developed; similarly, the thermal entry length tells us when the temperature profile became stable along the length of fluid flow. Table 3 indicates the correlation of hydrodynamic and thermal entry length for laminar and turbulent flow for fully developed conditions. For simplification, we are assuming the flow to be fully developed with an uncertainty of 5.2%.

Table 3: Correlation for entry length [13]

Type of flow	Hydrodynamic entry length	Thermal entry length	Equation number
Laminar	$0.05ReD_h$	$0.05ReD_h.Pr$	(25)
Turbulent	$10D_h$	$10D_h$	(26)

4. RESULTS AND DISCUSSION

For validation purposes, we perform the comparison study of our numerical model results with Andrejesdóttir et al.[7] experimental and numerical model with A_m equals to $11.7 * 10^{-3}$ m² and D_h equals to $5.2 * 10^{-3}$ m [7], Figure 2 shows the validation that is performed at TDS of 5 PPT with permeate bulk temperature of 294 K and at average Reynolds number between 6000 to 8200.

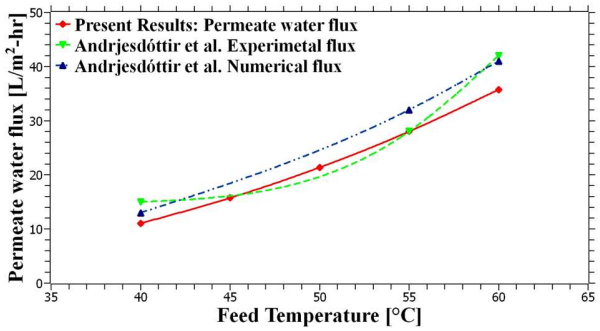

Figure 2: Validation performed at TDS of 5 PPT with T_{pb}=294 K and at average Reynolds number between 6000 to 8200 for different membranes

Figure 3 shows the validation that is performed at TDS of 15 PPT with permeates bulk temperature of 295 K and at average Reynolds number between 6000 to 8200. It indicates that the results our model obtained are closed to experimental results and are even better than the numerical results that Andrejesdóttir et al. achieved [7]. This shows that the permeate water flux is increasing with an increase in feed bulk temperature as expected due to an increase in driving force which increases exponentially with temperature

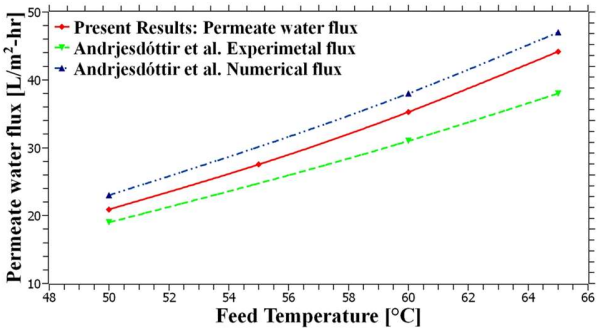

Figure 3: Validation performed at TDS of 15 PPT with T_{pb}=295 K and at average Reynolds number between 6000 to 8200 for different membranes

Figure 4 shows the variation of permeate water flux with the length of the membrane. The membrane length is varied between [0.4 – 2 m] for different types of membranes. Permeate water flux is calculated by taking the average temperature difference (feed and permeate membrane temperature) vapor pressure driving force at each point from starting to ending of the membrane. Results show that the permeate flux decreases with an increase in membrane length for all the membranes. As the feed water flow, the temperature drops along the length due to loss of HT, which results in loss of vapor pressure driving force at the tail end of membrane length.

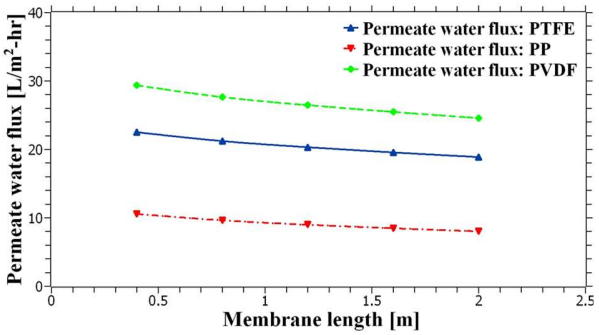

Figure 4: Effect of length for various membranes on flux at TDS of 10PPT with T_{fb}=333 K and T_{pb}=294 K

Figure 5 shows the variation in distilled mass flow rate with the length. The membrane length is varied between [0.4 – 2 m] for various membranes. Results show that distilled mass flow rate increases with increasing membrane length because as the membrane length increase, the area of the membrane also increases, and distilled mass flow rate is proportional to the area of the membrane; the curve is almost linear; it is due the reason the permeate water flux is almost constant as shown in figure 4.

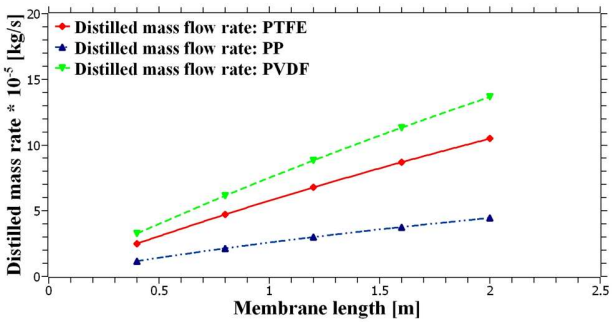

Figure 5: Effect of length for various membranes on the distilled mass rate at TDS of 10PPT with T_{fb}=333 K and T_{pb}=294 K

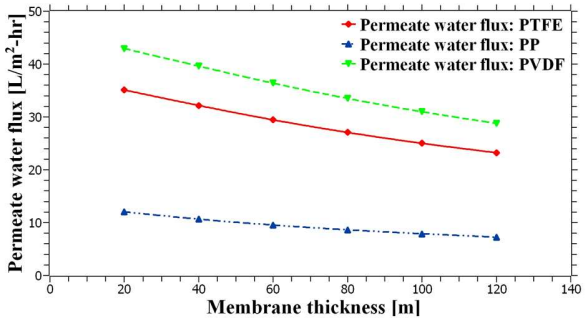

Figure 6: Permeate water flux as a function of membrane thickness at TDS of 10PPT with T_{fb}=333 K and T_{pb}=294 K for different membranes

The effect of Reynold's number on permeate water flux is shown in Figure 7. The Reynold's number is varied between [500-3500]. It shows that the water flux is increasing with the increment in Reynold's number in laminar as well as a turbulent region, but there is a sudden increase in water flux when the flow changes from laminar to turbulent; therefore, we can say that the transition phase is best for getting the optimum water flux because the further increase in Reynolds number is not advantages. After all, it will increase the water flux, but at the same time, it will increase the power consumption to increase that Reynolds number.

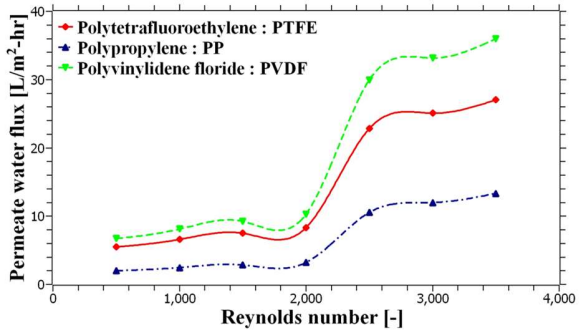

Figure 7: Effect of Reynold's number on permeate water flux at TDS of 10PPT with T_{fb}=333 K and T_{pb}=294 K for different membranes

Figure 8 shows the effect on flux in various regions of the world by keeping the temperature difference the same, i.e., 40 K for different membranes. The permeate bulk temperature is varied between [10-30°C], and the feed bulk temperature is changed between [50-70°C]. Still, their difference will remain constant for equal heat supply to predict the exact behavior of MD performance in different climate zones. It is found that the water flux is increasing with an increase in permeate bulk temperature as expected due to the rise in driving force that increases exponentially with temperature; therefore, the country with a high average annual temperature will get a higher permeate water flux compared to those with low annual average temperature.

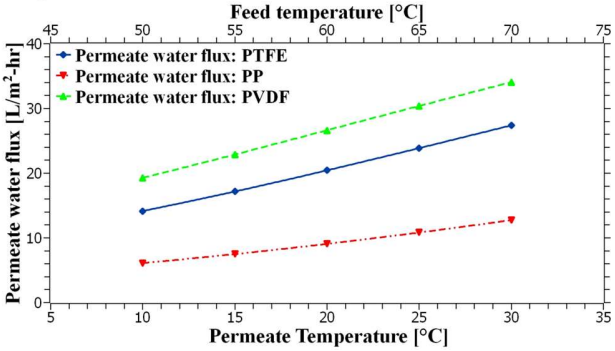

Figure 8: Effect on flux in various regions of the world by keeping the temperature difference the same, i.e., 40 K for different membranes

5. CONCLUSIONS

The present work shows the thermal analysis of DCMD in which a detailed fluid flow and heat transfer analysis is performed. The results of this paper are then validated. ϵ-NTU method is used to predict the temperature variation of feed and permeates bulk temperature at every membrane location along the length by considering the heat loss and temperature polarization effect. This paper studied the performance of DCMD and evaluated the permeate water flux at various climate conditions and getting the optimum result by performing the numerical mathematical modeling by varying various parameters like flow velocity, Reynold's number, membrane properties, the effect of different membranes on flux, and study shows that flux decreases with increase in membrane thickness and membrane length. Still, it increases with an increase in Reynold's number, i.e., feed velocity or mass flow rate of feed and permeate temperature by keeping the temperature difference identical, i.e., equal heat supply. DCMD performance can be improved by manufacturing the thinner membrane, using transition flow between laminar and turbulent, and by using the appropriate material, which provides better insulation at a reasonable cost.

ACKNOWLEDGEMENTS

The support received from the Department of Mechanical Engineering at IIT Ropar is gratefully acknowledged.

NOMENCLATURE

Symbols

A	Area	[m^2]

B	Mass transfer coefficient	[kg/m^2 -s-Pa]
C	Specific heat capacity	[J/kg-K]
D	Diameter	[m]
D_w	Diffusion coefficient of water	[m^2/s]
h	Heat transfer coefficient	[W/m^2-K]
H	Enthalpy	[J/kg]
J	Permeate water flux	[kg/m^2-s]
K	Thermal conductivity	[W/m-K]
L	Length	[m]
M	Molecular mass	[kg/mol]
P	Partial Pressure	[Pa]
Q	Heat transfer	[W]
r	Radius	[m]
R	Universal gas constant	[J/mol-K]
T	Temperature	[K]
U	Overall heat transfer coefficient	[W/ m^2-K]
v	Feed velocity	[m/s]
W	Wetted perimeter	[m]
X	Mole fraction	[-]

Subscript

f	Feed side
fb	Feed bulk
fm	Feed membrane
h	Hydraulic
i	Inlet
m	Membrane
o	Outlet
p	Permeate
pb	Permeate bulk
pm	Permeate membrane
T	Total
v	Vapor

Greek symbols

δ	Membrane thickness	[m]
ε	Porosity	[-]
ϵ	Effectiveness	[-]
τ	Tortuosity	[-]
λ	Mean free path	[m]
μ	Dynamic viscosity	[Pa-s]
ρ	Density	[kg/m^3]
φ	Coefficient of temperature polarization	[-]

Abbreviations

DCMD	Direct contact membrane distillation
DGM	Dusty gas model
HDH	Humidification-dehumidification
HT	Heat transfer
MD	Membrane distillation
NTU	Number of transfer unit
PPT	Parts per thousand
RO	Reverse osmosis
TDS	Total dissolved solids
UF	Ultrafiltration

REFERENCES

[1] Wash, R., 2002, "Water Security," Water Well J., 56(3), p. 58.

[2] Lawson, K. W., and Lloyd, D. R., 1997, "Membrane Distillation," J. Memb. Sci., 124(1), pp. 1–25.

[3] Gryta, M., Karakulski, K., and Morawski, A. W., 2001, "Purification of Oily Wastewater by Hybrid UF/MD," Water Res., 35(15), pp. 3665–3669.

[4] Criscuoli, A., and Drioli, E., 1999, "Energetic and Exergetic Analysis of an Integrated Membrane Desalination System," desalination, 124(1–3), pp. 243–249.

[5] Alkhudhiri, A., Darwish, N., and Hilal, N., 2012, "Membrane Distillation: A Comprehensive Review," desalination, 287, pp. 2–18.

[6] Nayar, K. G., Sharqawy, M. H., Banchik, L. D., and Lienhard, J. H., 2016, "Thermophysical Properties of Seawater: A Review and New Correlations That Include Pressure Dependence," desalination, 390, pp. 1–24.

[7] Andrjesdóttir, Ó., Ong, C. L., Nabavi, M., Paredes, S., Khalil, A. S. G., Michel, B., and Poulikakos, D., 2013, "An Experimentally Optimized Model for Heat and Mass Transfer in Direct Contact Membrane Distillation," Int. J. Heat Mass Transf., 66, pp. 855–867.

[8] Qtaishat, M., Matsuura, T., Kruczek, B., and Khayet, M., 2008, "Heat and Mass Transfer Analysis in Direct Contact Membrane Distillation," desalination, 219(1–3), pp. 272–292.

[9] Boubakri, A., Hafiane, A., and Bouguecha, S. A. T., 2017, "Direct Contact Membrane Distillation: Capability to Desalt Raw Water," Arab. J. Chem., 10, pp. S3475–S3481.

[10] Fan, H., and Peng, Y., 2012, "Application of PVDF Membranes in Desalination and Comparison of the VMD and DCMD Processes," Chem. Eng. Sci., 79, pp. 94–102.

[11] Schofield, R. W., Fane, A. G., and Fell, C. J. D., 1987, "Heat and Mass Transfer in Membrane Distillation," J. Memb. Sci., 33(3), pp. 299–313.

[12] Phattaranawik, J., Jiraratananon, R., and Fane, A. G., 2003, "Effect of Pore Size Distribution and Air Flux on Mass Transport in Direct Contact Membrane Distillation," J. Memb. Sci., 215(1–2), pp. 75–85.

[13] Cengel, Y. a., 2006, *Heat and Mass Transfer: A Practical Approach*.

[14] Phattaranawik, J., Jiraratananon, R., and Fane, A. G., 2003, "Heat Transport and Membrane Distillation Coefficients in Direct Contact Membrane Distillation," J. Memb. Sci., 212(1–2), pp. 177–193.

[15] Wu, H. Y., Tay, M., and Field, R. W., 2016, "Novel Method for the Design and Assessment of Direct Contact Membrane Distillation Modules," J. Memb. Sci., 513, pp. 260–269.